

We are IntechOpen, the world's leading publisher of Open Access books Built by scientists, for scientists

4,800

Open access books available

122,000

International authors and editors

135M

Downloads

Our authors are among the

154

Countries delivered to

TOP 1%

most cited scientists

12.2%

Contributors from top 500 universities



WEB OF SCIENCE™

Selection of our books indexed in the Book Citation Index
in Web of Science™ Core Collection (BKCI)

Interested in publishing with us?
Contact book.department@intechopen.com

Numbers displayed above are based on latest data collected.
For more information visit www.intechopen.com



Low-Cost (PM Less) Wide-Speed-Range-Operation Generators

*Sorin Ioan Deaconu, Feifei Bu, Marcel Topor,
Lucian Nicolae Tutelea and Nicolae Muntean*

Abstract

This chapter presents a novel dual stator-winding induction generator (DSWIG) system for wind power generation, and an optimal scheme to decrease the capacity of static excitation converter (SEC) is also given. The main result is represented by the finding that reactive excitation power released by the excitation capacitor and SEC is not only correlated to generator parameters, speed range, and load but also affected by wind turbine power curve. This chapter also investigates the optimal excitation capacitor selection process. Considering the objective of minimizing the capacity of SEC, several methods are tested here to identify an appropriate excitation capacitor value. Using the general d-q model in the stator-voltage-orientation synchronous frame of the DSWIG control algorithm and model of SEC, a decoupling control strategy using the space vector modulation (SVM) is determined for the six-phase DSWIG. Based on the obtained models, the computer simulation and experimental investigations of a test prototype orated at 18 kW with six stator phases and three-phase wound rotor DSWIG wind power system were carried out to validate the optimal solution for the system. The matching results (simulation and teststand measurements) demonstrate the correctness and effectiveness of this optimization scheme.

Keywords: DSWIG, excitation capacitor, static excitation controller, space vector modulation

1. Introduction

In the latest 30 years, due to the depletion of fossil fuels and the increasing environmental concerns and consequently strict regulations, wind energy has become one of the most widely integrated renewable resources, attracting more and more investments and scientific attention. Statistically by the year of 2012, about 282,430 MW of wind power were installed all over the world [1], and it is targeted that in 2030 a percent equal to 10–20% of the global electrical energy used will be produced by wind farms [2]. As a result of the general orientation toward a higher degree of wind energy generation in the grid, there is a strong direction to install the wind farms offshore. The reason is represented by the fact that the wind resource has a better availability and the problems of noise pollution and the effect on the site can be handled without great difficulty [3].

The large offshore wind farms will require a transmission of energy produced from the offshore wind farm to the grid connection point. The general solution is to have a high-voltage ac (HVAC) or high-voltage dc (HVDC) transmission. Usually, offshore wind farms are located at distances <120 km from the shore. This wind farms have the capacity <150 MW which is possible to be connected to the grid using an HVAC transmission, whereas at longer distances and/or with higher capacity, only the HVDC transmission is recommended mainly due of its economic and technical advantages [4].

There are a large number of topologies of electric machines which can be used as generators for wind power systems, among which we may include the synchronous machine, induction machine, switched reluctance machine, etc. [5, 6]. However, the very strict requirements to reach high performance and high reliability are the development of the large and long-distance offshore wind farms operating with the HVDC transmission. In order to have this, a number of technical proposals have been considered to be promising [5, 7–10]. The large majority of them are built on the permanent magnet synchronous generator (PMSG) topology and on the doubly fed induction generator (DFIG) topology. It is considered that the PMSG-based generator wind turbines feeding the load through a dc bus voltage is appropriate for the HVDC transmission between the farm and shore grid, Even though this type of generators has a higher power density and efficiency, they have a cost disadvantage given to the rapid increase of rare-earth material price. This rather simple solution requests a full-rated power converter which is disequilibrium in the cost of installment and operation between the generator and the power converter [9]. In contrast to the DFIG, it requires power converter representing only 25% of the generator rated power (if we consider a limited speed range of 0.75–1.25 p.u.). Of course the presence of slip rings and brushes in order to supply power to the rotor side leads to a rise of the maintenance cost. If we consider a HVDC transmission, a voltage-source converter, or a line-commutated converter, it has to be included since the voltage output of the DFIG is three-phase constant ac voltage and frequency [10].

2. State of the art in dual stator-winding induction generators (DSWIG)

The rotor cage-type induction generator (IG) constitutes an excellent choice for building wind turbine generators. It has many advantages for wind power applications, such as natural brushless construction, low maintenance request, good overload protection capability, and many other excellent features [11]. For traditional IG systems, one important disadvantage is the difficulty to realize regulation of excitation reactive power and the poor output voltage dynamic performance under the variations of load and speed, which limits their extended applications. With the rapid development of power electronics and electric machine control strategies, many improved topologies have been proposed to circumvent the aforementioned problems [11–14]. We can mention here at least one which is represented by the connection of a dc-ac voltage-source inverter in parallel or series with the loads to provide variable excitation reactive power. This solution has facilitated a performant control of IG systems, but most of these improved solutions will require a certain amount of injected harmonics into the load current and will have as side effect induced the output voltage ripple.

A step forward into the problem to effectively control the output voltage and eliminate/decrease the harmonics generated from power commutation, a dual stator-winding induction generator (DSWIG) with a static excitation converter (SEC) as proposed in [15]. Under the variable speed and load regime in order to get constant frequency and constant voltage, this system suffers from the complexity or

low efficiency due to the use of a discharge resistance or battery [16]. For power systems operating in aircrafts, ships, and wind power applications, a DSWIG-based dc generating system with one or more diode rectifiers connected to the power winding is recently explored in [16–19]. This kind of system is characterized by a good performance of the dc voltage output with a small-size power converter capable of operating under the dynamic variable speed and load, which indicates the fact that it can also be used in wind power systems, especially as a suitable solution for the offshore wind farms using the HVDC transmission technology.

The prime mover in wind power system is the wind turbine. The output power of it is not only related to the wind speed but also has much to do with the rotor speed, turbine speed, rotor blade tilt, rotor blade pitch angle size and shape of turbine, swept area of turbine blades, rotor geometry whether it is a HAWT or a VAWT, and wind speed turbulences which constitute the mathematical model of the wind turbine. The characteristics of the wind turbine depend on the type of prime mover. The turbine position and its nonlinearities should be taken into consideration seriously when designing or controlling a wind power system. Nevertheless, the long list of research papers written for the type of DSWIG is concentrated primarily upon the control and optimization for the abovementioned power system configuration. When the DSWIG system is powered by the wind turbine, if we consider the capacity optimization problem for SEC, in our opinion these available optimal schemes mentioned in literature are not appropriate for the DSWIG used in wind power farm.

As a consequence of the existing constraints regarding the overall cost and volume, the capacity of the chosen SEC is one of the important elements of the design of wind power system. In this chapter, the optimal sizing algorithm of excitation capacitor designed to decrease the capacity of SEC for DSWIG wind power system is presented. We have considered a number of methods to be investigated and employed to identify the optimal excitation capacitor in a step-by-step procedure. The simulation and experimental results from the tests performed on 18 kW six-phase/three-phase DSWIG wind power system prototype supplying a rectifier load for dc voltage output are shown for comparison and validation.

3. System topology and model

3.1 DSWIG wind power system

The configuration of a prototype six-phase/three-phase DSWIG wind power system is shown in **Figure 1**.

The stator winding consists in a two set of shifted windings which are located in the stator slots in this generator. The first winding referred to as ix-phase power winding, is built using two three-phase star windings shifted by a 30-degree electric angle, and supplies power to the dc load via a six-phase bridge rectifier. The second winding, identified as a three-phase control winding, is connected to the static excitation controller (SEC). A standard squirrel-cage rotor is used by this generator. The two windings (power and control) have the same number of poles, so they share the same working frequency. It has been found that [1] because there is no electric connection between the two sets of windings, the electromagnetic compatibility (EMC) of the system is improved greatly.

Wind energy is transformed into mechanical energy and therefore into dc power by the wind turbine and DSWIG, respectively. The power winding will transfer the generated power to the dc load through the rectifiers connected at the grid side. Using two three-phase diode bridges connected in parallel or series, it is possible to supply a dc bus or a dc load.

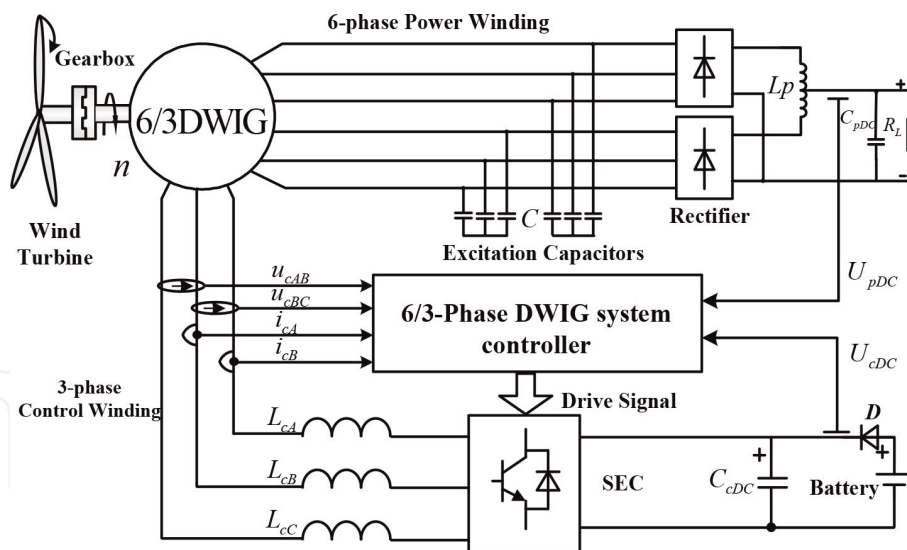


Figure 1.
Six-phase/three-phase DSWIG wind power system.

In this chapter, we have considered that the parallel connection of the windings with an interphase reactor is selected. In order to provide partial reactive power for the excitation of the generator, a fixed excitation capacitors bank to the terminal of six-phase power winding. In case of the control winding, a switch-mode pulse-width modulation (PWM) voltage-source SEC is used to produce variable reactive power to secure the performance of dc voltage output according to the different working conditions. In this configuration, the dc bus capacitor behaves as a voltage source of SEC.

In this rather simple electric power generation system, the prime mover is the wind turbine. As we may know, the output mechanical energy of the wind turbine varies with the wind and rotor speed besides many other factors. According to the Betz law, the rotor speed should be constantly dynamically adapted with the wind to capture more wind power, which can be implemented by the control of output power [20, 21]. As a consequence the system should naturally have the capability to self-adapt to the variations of speed and load, which will conduct to a large change of the reactive excitation power produced by the fixed excitation capacitors and to a great variation of the capacity of SEC. However, there is a possible solution if the excitation capacitors connected to the power winding were optimally selected. In this case the capacity of SEC will be decreased considerably, which will lead to a low-cost power and compact-size generation system. Therefore, the optimal algorithm for the selection of the excitation capacitor is very important for the DSWIG applied in wind power system.

In this type of system, the objective is to have the dc bus voltage of power winding U_{pDC} constant. In order to have this condition fulfilled, the control objectives need to consider the speed and load variations. This implies that we need to maintain U_{cDC} , the dc bus voltage of SEC, stable as this is the basic condition for the normal work of SEC. According to the instantaneous power theory, it is possible to control both the active and reactive components of the control winding current separately, and in order to maintain a direct control of the generator, instantaneous active and reactive power is used in order to meet the control objectives [22]. In this chapter, we present a mathematical model of SEC developed using the d-q frame with the reference orientation being synchronous to the stator voltage. In this work, the closed interconnection between the d and q axis quantities is considered, and based on this, the rather new control strategy with decoupling using SVM for the DSWIG wind power generator is introduced.

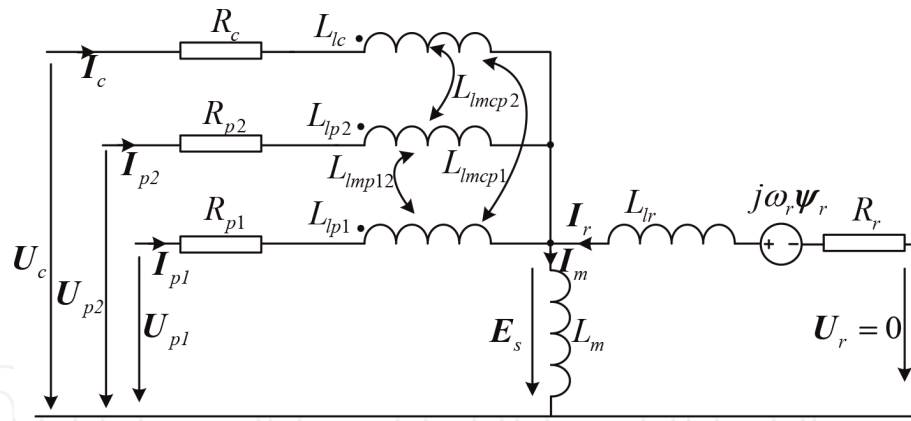


Figure 2.
 The equivalent circuit of six-phase/three-phase DSWIG in stationary reference frame.

3.2 DSWIG model

The equivalent circuit schematic of six-phase/three-phase DSWIG in the stationary reference frame is shown in **Figure 2**. In this representation, the equivalent circuit parameters of the rotor winding and the control winding are referred to the power winding. The dynamic model of the generator expressed in the complex variable form can be written as follows [15]:

The voltage equations are written as

$$\begin{cases} U_{p1} = R_{p1}I_{p1} + d\psi_{p1}/dt \\ U_{p2} = R_{p2}I_{p2} + d\psi_{p2}/dt \\ U_c = R_cI_c + d\psi_c/dt \\ U_r = R_rI_r - j\omega_r\psi_r + d\psi_r/dt \end{cases} \quad (1)$$

where

$$\begin{cases} \psi_{p1} = L_{p1}I_{p1} + L_{lmp12}I_{p2} + L_{lmcp1}I_c + L_mI_r \\ \psi_{p2} = L_{lmp12}I_{p1} + L_{p2}I_{p2} + L_{lmcp2}I_c + L_mI_r \\ \psi_c = L_{lmcp1}I_{p1} + L_{lmcp2}I_{p2} + L_cI_c + L_mI_r \\ \psi_r = L_mI_{p1} + L_mI_{p2} + L_mI_c + L_rI_r \end{cases} \quad (2)$$

$L_c = L_m + L_{lc}$; $L_r = L_m + L_{lr}$; $L_{p1} = L_{p2} = L_m + L_{lp}$; L_{lp} , L_{lc} , and L_{lr} represent the leakage inductance corresponding to the power winding, the control winding, and, respectively, the rotor; L_{lm} represents the mutual leakage inductance between the stator windings; and L_m is the magnetizing inductance. The variables U , I , and ψ represent the voltage, current, and flux; their subscript letters p , c , and r indicate the correspondence to the stator power winding, stator control winding, and rotor. Numbers (1) and (2) indicate the first and second set of power winding distinctly. The derivative of the above variables is written by d/dt , and ω_r is the angular rotor electrical frequency.

4. Principle of design with optimization

4.1 Wind turbine characteristics

The power captured by the wind turbine is expressed by Eq. (3), which is a function depending on the blade shape, the pitch angle, the radius, and the rotor speed of rotation [20]:

$$P_T = \frac{1}{2} \pi \rho R^2 C_p(\lambda, \beta) V^3 \quad (3)$$

where ρ is the air density (in kg/m^3), R is the blade radius (in m), β is the pitch angle (in degrees), $C_p(\lambda, \beta)$ is the wind turbine power coefficient, and V is the wind speed (in m/s). λ is the tip-speed ratio, defined as

$$\lambda = \frac{2\pi n R}{60V} \quad (4)$$

where n is the rotor speed (in rev/min).

The general wind turbine power curves for various wind speeds are shown in **Figure 3**. From this it can be easily noticed that, for each wind speed, there exists a maximum power point in the wind turbine output. This point is located on the power versus rotating speed characteristic. P_{opt} , in **Figure 3** the line connecting this point, is the maximum power curve which is the line coupling all the maximum power points obtained at different wind speeds.

The maximum power point is obtained for the wind turbine having a fixed pitch angle (the β is fixed), when the tip-speed ratio λ equals λ_{opt} , and the wind turbine power coefficient C_p is equal to maximum. In this condition, the maximum output power can be written as

$$P_{T_{max}} = \frac{1}{2} \pi \rho R^2 \left(\frac{2\pi R}{60\lambda_{opt}} \right)^3 C_{p_{max}} n^3 \quad (5)$$

$$\lambda_{opt} = \frac{2\pi R}{60} \cdot \frac{n_{opt}}{V} \quad (6)$$

One may need to maximize the output power of wind turbine within the range of variation of wind speed. For this reason the rotor speed must be kept proportional with the wind speed to insure the value of the tip-speed ratio constant for all the maximum power point according to Eqs. (5) and (6). The control of the generator requires the use of the maximum power point tracking (MPPT) method for the wind turbine operating at a variable speed. The process can be implemented in advanced controller in order to strength optimal power generation output, like in [20, 21].

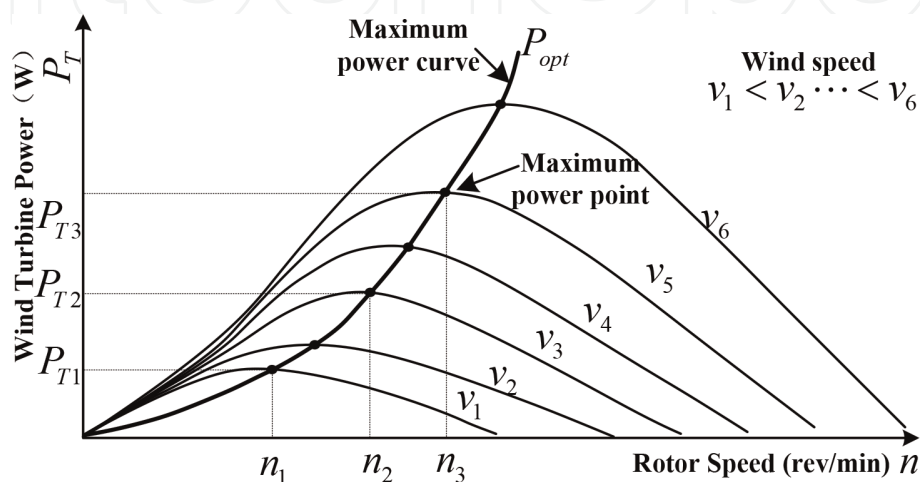


Figure 3.
Wind turbine power curves for various wind speeds.

4.2 The optimal selection algorithm of excitation capacitor

Considering the various wind speed and wind turbine power curve areas, the operation of DSWIG wind power system can be divided into four stages A-B-C-D-E, as shown in **Figure 4**.

4.2.1 Stage I: segment A-B: the initialization sequence of wind power system

The process initiates when the wind speed is greater than the start-up value. At this moment the rotor blades initiate the spinning, and the rotor speed slowly increases, as shown in A-B segment in **Figure 4**. The generator will not provide any power during this sequence.

4.2.2 Stage II: segment B-C: the voltage buildup sequence of DSWIG wind power system

In this stage, the system is initiating the voltage generation when the minimum speed need is obtained. During this sequence, the reactive power needed for excitation is supplied through the excitation capacitor and SEC simultaneously. In addition to this, it is necessary to maintain the dc-side capacitor voltage constant with the SEC supplying the part of the active power required for charging, which is essential to the normal operation of the system [22]. The generating mode is possible after the nominal excitation voltage is reached.

4.2.3 Stage III: segment C-D: the operation of system within the range of low wind speed

When the cut-in speed is reached, the generator begins to produce enough power in order to begin the export. The rotor speed is still low due to the small wind speed. As a result, the output voltage of rectifier connected to the power winding cannot reach the nominal value. One may notice that the output power is related to the cube of the wind speed, and, thus, it is very small in this wind speed operating zone. In order to take advantage of this part of the wind curve characteristic, we consider the voltage pump-up theory as it is presented in [23]. When the voltage in the DC bus of SEC is reaching the reference value, the output power is mainly generated through the SEC from the control winding. The matching equations of wind speed, rotor speed, and output power are represented under the form of a curved line labeled B-C in **Figure 4**.

4.2.4 Stage IV: segment D-E: the large wind speed domain regime of the wind power system

When the value of speed of the wind system is relatively stable within the large wind region, the rectified output voltage can match the nominal value, and the

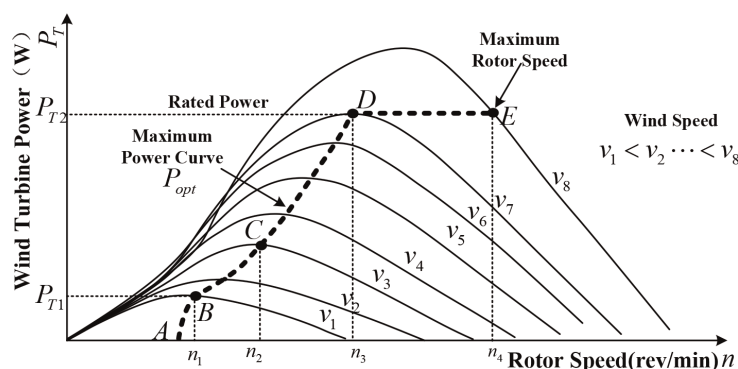


Figure 4.
 The characteristic of DSWIG wind power system variable wind speed.

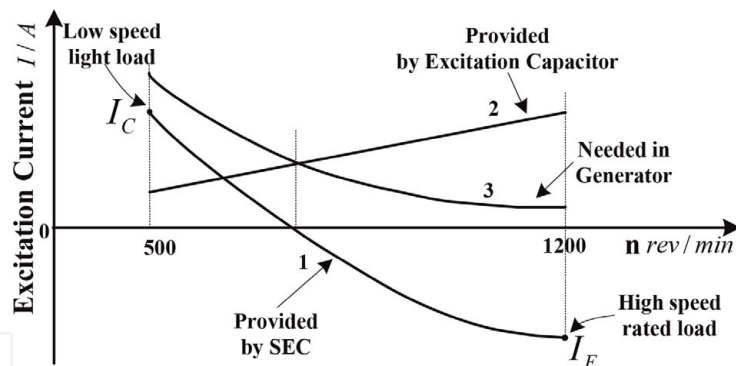


Figure 5. The change of excitation current in CDE segment in large wind speed zone.

wind power generator system can provide energy at maximum power under different wind speeds (i.e., P_{opt} in **Figure 4**). Since constant output voltage is needed, the reactive power needed for generator excitation provided by the excitation capacitors is not sufficient, and for this reason, the remaining share is given by the SEC. When the wind is accelerating steadily, the wind turbine speeds up, so the reactive excitation power provided by the excitation capacitor also increases; thus, the reactive energy supplied by the SEC decreases accordingly. During the speed up, the SEC gets more reactive excitation power from the generator instead of providing it. If the wind speed slows down beyond the rated value, some correcting actions need to be performed in order to limit the output power of the wind turbine [10]. A first measure is the modification of the pitch angle. Another measure is to reduce the magnetization field. The field should be weakened in order to be sure that the constant output power of the generator is kept. This process is represented by the CDE segment in **Figure 4** where the change of excitation current is exposed in **Figure 5**.

Curve 1 in **Figure 5** presents the control winding current variation when the generator operates within the range of CDE area. When the current value is positive, the SEC provides insufficient reactive power to the generator; and when the value is negative, the SEC there is an excessive reactive excitation which imposes a correction. The maximum positive current I_C in control winding occurs at low-speed, light-load situations (as it can be noticed from **Figure 5**) (corresponding to point C in **Figure 4**), while the negative minimal current I_E occurs at high-speed rated-load moments (corresponding to point E in **Figure 4**).

In this chapter, the sizing equations based on mathematical model and simulation methods are used to obtain an suitable the excitation capacitor value, capable of maintaining the current flowing through the control winding at a variable speed and load regime following strictly the law, $|I_C| = |I_E|$. Thus, the minimal capacity of SEC is found for the DSWIG wind power system.

4.3 The selection of optimal excitation capacitor for an 18 kW six-phase/three-phase DSWIG wind power system

4.3.1 Optimal excitation capacitor identification using the graphic method

The equivalent circuit parameters of the prototype 18 kW multiphase stator windings with six-phase/three-phase DSWIG studied in this paper are given in Appendix. The waveforms of the control winding current I_c obtained using various excitation capacitors are analyzed, and the results are shown in **Figure 6**. In this figure, two different situations regarding the low-speed, light-load and the high-

speed rated-load moments were investigated. The shape of curve I_{c1} synthesizes the effect the control winding current at 500 rev/min with 4 kW (the corresponding maximum output power to this speed). Curve I_{c2} illustrates the effect of the control winding current at 1200 rev/min with 18 kW. Output of the excitation capacitor value ranges from $10\mu\text{F}$ to $140\mu\text{F}$.

Curve $-I_{c2}$ is the symmetrical about the X-axis with curve corresponding the I_{c2} . The maximum absolute value of the control winding positive and negative current is equal in this process, and thus the intersection of curve I_{c1} and $-I_{c2}$ is point O, which is indicated that the excitation capacitor is $70\mu\text{F}$. In few words, the optimal excitation capacitor can be easily determined by this graphic method.

4.3.2 Optimal value of the excitation capacitor identification using the iterative approach

Using a value $70\mu\text{F}$ as the optimal excitation capacitor, the variation of control winding current is rendered under the form of curve 1 in Figure 7. In this graphic, the maximum positive current is $I_C = 8\text{A}$ and the minimal negative current is

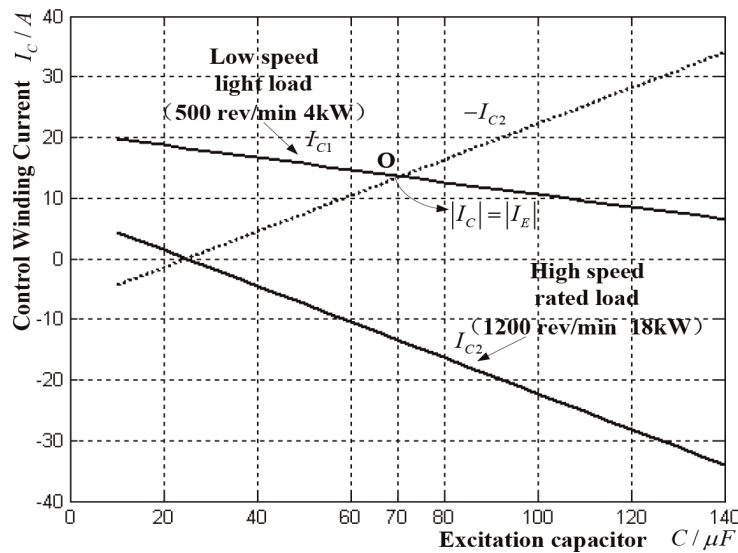


Figure 6.
 The influence of various excitation capacitors on the control winding current.

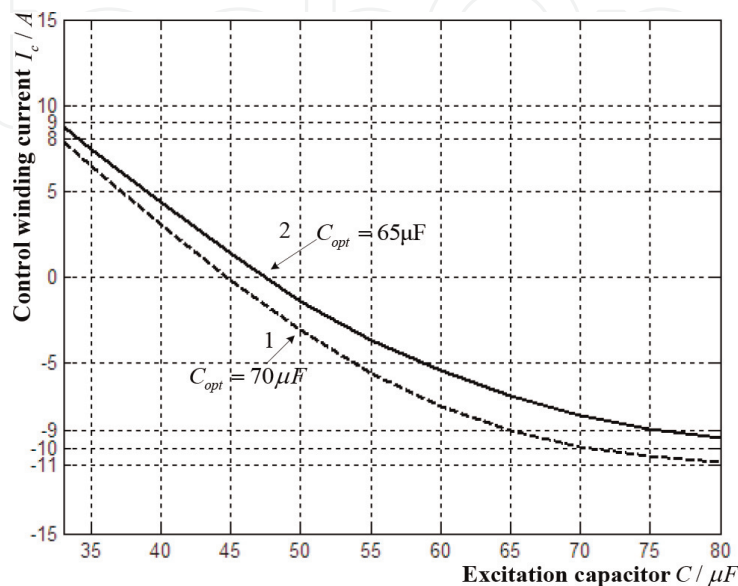


Figure 7.
 The law of control winding current based on the optimal excitation capacitor.

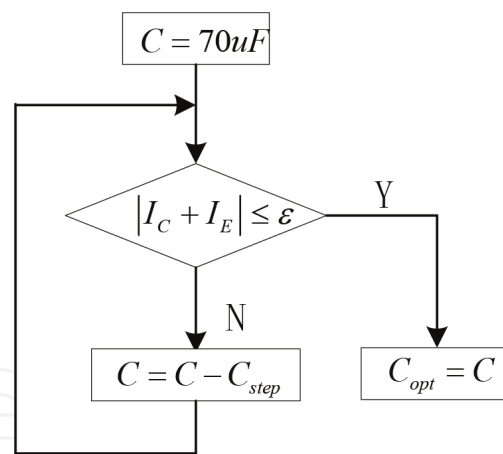


Figure 8.
The sketch map of iterative algorithm.

$I_E = -10A$. This value implies that the excitation capacitor is somewhat large, requiring a reduction of the value.

The graphic method is based on the identification of the two curves intersection graphically, where the intersection denotes the optimal excitation capacitor. Although some errors are expected, the result can be considered as a reference value. Therefore, this value can be established as the initial guess value for the recursive method. In this chapter, in order to identify the optimum value recursive algorithm, the capacitance value of the excitation capacitor is viewed as an optimization variable, $|I_C + I_E| \leq \varepsilon$ as the optimization constrain target, and the initial guess of the capacitance equal to 70 μF is the starting initial value.

The recursive algorithm flowchart is shown in **Figure 8**. The optimal value is obtained after several iterations, and after the target reaches the optimal excitation capacitor, $C_{opt} = 65\mu F$ is obtained. Considering this as the optimal value of the excitation capacitor, we obtain curve 2 in **Figure 7** is accomplished. Through the entire optimization process, the absolute values of maximum and minimum currents flowing through the control winding are both about 9A. In fact, I_c echoes the capability of SEC to provide excitation for the generator. By means of a synthesis of graphical and recursive methods, the optimal value for excitation capacitor can be found to apprehend the capacitor value minimization of SEC for the wind power system with DSWIG generator connected to a passive resistance load.

5. Control strategies

5.1 A synthetic analysis of the control algorithms for the multiphase DSWIG system

According to the analysis depicted in Ref. [22], the two sets of windings share the same air-gap flux; thus any change of control winding flux will cause the variation of air-gap flux, which can determine a reaction in the DC-bus voltage of power winding U_{pDC} . Due to the power loss occurring inside the SEC, U_{cDC} would be faded. In this way, U_{cDC} must be strictly controlled to enforce the standard work condition of SEC, which can be further realized by the controller of the electromagnetic torque produced by control winding T_{emc} . The relationship between corresponding parameters can be expressed as follows:

$$\begin{cases} \psi_c \rightarrow U_{pDC} \\ T_{emc} \rightarrow U_{cDC} \end{cases} \quad (7)$$

Based on the instantaneous power theory [24], the control winding instantaneous power can be stated as in Eq. (8) in the d-q coordinate frame referencing the control winding terminal voltage vector U_c :

$$\begin{cases} p_c = \omega_1 \psi_c i_{cd} \\ q_c = \omega_1 \psi_c i_{cq} \end{cases} \quad (8)$$

This way we can obtain the following equality:

$$\frac{p_c}{q_c} = \frac{i_{cd}}{i_{cq}} \quad (9)$$

where p_c and q_c denote the instantaneous active and reactive power generated by the current in the control winding, respectively. i_{cd} and i_{cq} are the d-q components of control winding current i_c . ω_1 is the angular stator electrical frequency.

Eq. (8) shows that the q component of control winding current, i_{cq} , is generating the instantaneous reactive power q_c , while i_{cd} generates p_c , namely:

$$\begin{cases} i_{cd} \rightarrow p_c \\ i_{cq} \rightarrow q_c \end{cases} \quad (10)$$

From equation [22], in variable speed and load regime, the management of T_{emc} can be realized by the control of two components, namely p_c and q_c , which can fine-tune the control winding flux. Briefly, the following relationship can be obtained:

$$\begin{cases} p_c \rightarrow T_{emc} \\ q_c \rightarrow \psi_c \end{cases} \quad (11)$$

As it is stated above, the control algorithms for the DSWIG power generation system functioning in variable rotor speed and load regime driven by wind power turbine may be written as it follows according to Eqs. (7), (10), and (11):

$$i_c \xrightarrow{U_c\text{-oriented}} \begin{cases} i_{cd} \rightarrow p_c \rightarrow T_{emc} \rightarrow U_{cDC} \\ i_{cq} \rightarrow q_c \rightarrow \psi_c \rightarrow U_{pDC} \end{cases} \quad (12)$$

5.2 The mathematical equivalent model for the DSWIG system

In order to simplify the equations, only the fundamental component of voltage is considered, and the hysteresis and eddy current losses are disregarded. Using this assumptions DSWIG can be considered as a voltage source seen from the side of the control winding [25]. **Figure 9** shows the equivalent circuit of the DSWIG system in simplified vector form.

Using the aforementioned equations, the voltage equation of the equivalent circuit can be yielded as

$$U_m = L \frac{dI_c}{dt} + U_c \quad (13)$$

Eq. (13) can be rewritten using the $\alpha - \beta$ reference frame:

$$\begin{bmatrix} U_{m\alpha} \\ U_{m\beta} \end{bmatrix} = L \frac{d}{dt} \begin{bmatrix} i_{c\alpha} \\ i_{c\beta} \end{bmatrix} + \begin{bmatrix} U_{c\alpha} \\ U_{c\beta} \end{bmatrix} \quad (14)$$

If the d-q coordinates is referenced to the control winding terminal voltage vector U_c , shown in **Figure 10**, Eq. (14) can be transformed into the d-q reference frame coordinates:

$$\begin{bmatrix} U_{md} \\ U_{mq} \end{bmatrix} = L \frac{d}{dt} \begin{bmatrix} i_{cd} \\ i_{cq} \end{bmatrix} + L\omega_1 \begin{bmatrix} -i_{cq} \\ i_{cd} \end{bmatrix} + \begin{bmatrix} U_{cd} \\ U_{cq} \end{bmatrix} \quad (15)$$

where

$$\begin{bmatrix} U_{cd} \\ U_{cq} \end{bmatrix} = \begin{bmatrix} U_c \\ 0 \end{bmatrix} \quad (16)$$

where U_c is the magnitude of U_c , and Eq. (17) can be obtained by the joint of Eqs. (15) and (16):

$$\begin{bmatrix} U_{md} \\ U_{mq} \end{bmatrix} = L \frac{d}{dt} \begin{bmatrix} i_{cd} \\ i_{cq} \end{bmatrix} + L\omega_1 \begin{bmatrix} -i_{cq} \\ i_{cd} \end{bmatrix} + \begin{bmatrix} U_c \\ 0 \end{bmatrix} \quad (17)$$

In this way, the control winding current in the U_c -oriented d-q coordinates can be written as

$$\begin{cases} i_{cd} = \int \frac{U_{md} + L\omega_1 i_{cq} - U_c}{L} dt \\ i_{cq} = \int \frac{U_{mq} + L\omega_1 i_{cd}}{L} dt \end{cases} \quad (18)$$

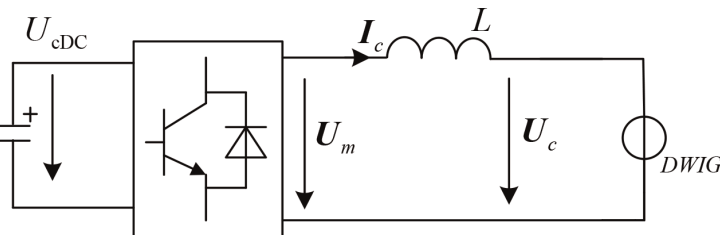


Figure 9.
The equivalent circuit of the DSWIG system.

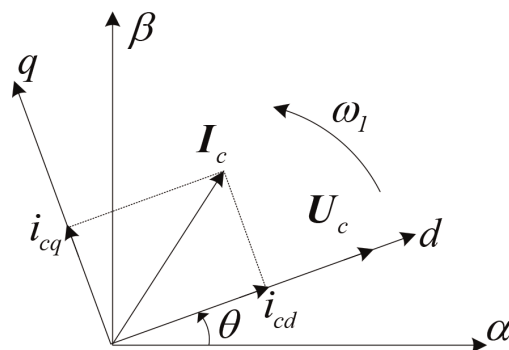


Figure 10.
The stator voltage orientation of the control winding.

Based on the analysis presented previously, we may develop the mathematical equivalent model of control winding connected with SEC. This model is specified in **Figure 11**. The d-q components of I_c , i_{cd} , and i_{cq} will control the instantaneous active and reactive power, respectively.

This controller can be implemented by usually making use of PI-type current controller to make the control winding current track the command current. However, Eq. (18) implies that there is a cross coupling between the d and q channels, which obviously if we consider **Figure 11**. This cross coupling will decline the static and dynamic performance.

5.3 Decoupling control strategy using space vector modulation SVM

A decoupling control strategy using SVM for the DSWIG wind power system is presented in **Figure 12**.

The command voltage components are provided given as function depending on the two-axis PI regulators output and the inductance:

$$\begin{cases} U_{md}^{*de} = PI(i_{cd}, i_{cd}^*) - L\omega_1 i_{cq} + U_c \\ U_{mq}^{*de} = PI(i_{cq}, i_{cq}^*) + L\omega_1 i_{cd} \end{cases} \quad (19)$$

where U_{md}^{*de} and U_{mq}^{*de} are used for the SEC by the SVM; Eq. (19) can be converted into the following equation:

$$\begin{cases} PI(i_{cd}, i_{cd}^*) - L\omega_1 i_{cq} + U_c = L \frac{di_{cd}}{dt} - L\omega_1 i_{cq} + U_c \\ PI(i_{cq}, i_{cq}^*) + L\omega_1 i_{cd} = L \frac{di_{cq}}{dt} + L\omega_1 i_{cd} \end{cases} \quad (20)$$

This expression can simplify into an integral form:

$$\begin{cases} i_{cd} = \int \frac{PI(i_{cd}, i_{cd}^*)}{L} dt \\ i_{cq} = \int \frac{PI(i_{cq}, i_{cq}^*)}{L} dt \end{cases} \quad (21)$$

Equation (21) implies that it is possible to linearize the relationship between the input and output of the model of control winding including SEC using the

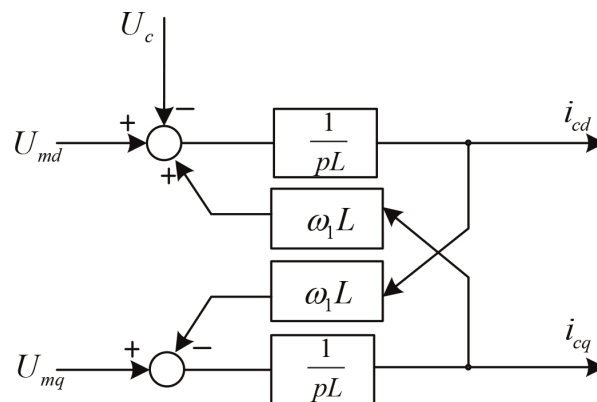


Figure 11.
 The model of control winding including SEC.

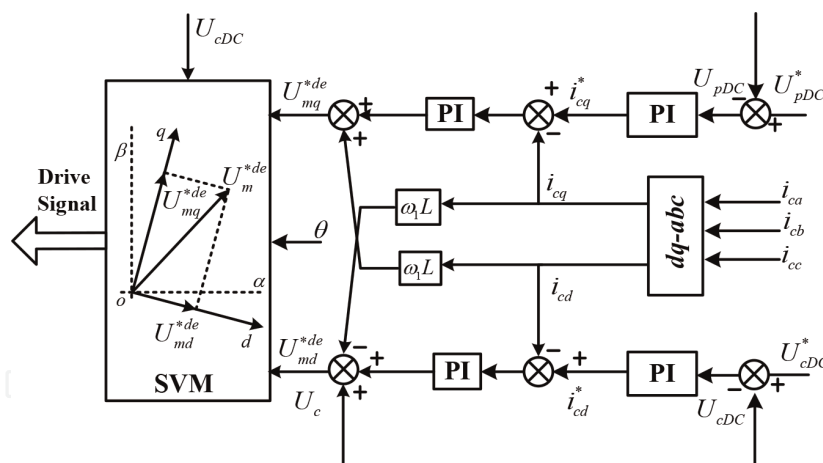


Figure 12.
The decoupling control strategy using SVM for six-phase/three-phase DSWIG system.

command voltage with corresponding decoupling elements. This way, the system naturally guarantees that the decoupling control strategy is effective transforming the equations into a first-order linear dynamic system. Using the command voltage U_{md}^{*de} and U_{mq}^{*de} , the SVM is employed to generate the switching signals for the power switches.

6. Simulation and experimental results

6.1 Simulation results

Theoretically, the optimal excitation capacitor obtained from the sizing algorithms corresponds to a generator loaded only with a resistive load, excluding the influence of rectifier load. But in practice the nonlinear influence of rectifier load for the whole system cannot be fully neglected.

The simulation model for six-phase/three-phase DSWIG wind power generation system is built based on the decoupling control strategy using SVM presented above. The equations were coded into a complex model with the help of MATLAB/Simulink to additionally fine-tune the value of the optimal excitation capacitor.

In this simulation model, the suitable tunings for C_{opt} are made, when $C_{opt} = 62\mu F$. The simulation results are shown in **Figure 13**.

When the rotor speed is inferior to the value of 300 rev/min, there is no voltage at the output of the generator, as shown in phase 1 in **Figure 13**. If the speed is growing over 300 rev/min, the system begins to build up the voltage. From phase 2 in **Figure 13**, it can be noticed that the corresponding dc bus voltage U_{pDC} and U_{cDC} will raise progressively with the development of line-to-line voltage and line current in the control winding. As a consequence of the low speed, the voltage in the dc bus output of power winding U_{pDC} cannot increase and maintain itself up to the specified value 600 V. On the contrary, the U_{cDC} can yield 600 V due to the voltage pumping-up capability of control winding. The output power is small in phase 3 in **Figure 13** as it may be seen in the power curve. Consequently, the power is provided from control winding side somewhat from the power winding over SEC. With the additional growth of the rotor speed, the dc voltage of power winding-rectified output can arise up to 600 V of the specified value of the generation system. At this situation, the state change of this DSWIG system is engaged. The control winding output generated power is surpassed by the power output of the

power winding. In phase 4 in **Figure 13**, this changeover is exposed. The modification of U_{pDC} raising from 200 to 600 V can be seen, while U_{cDC} is preserved at 600 V constantly.

After this transient state, the rotor speed ramps up from 500 to 1200 rev/min and stays at 1200 rev/min afterward, as shown in phase 5 in **Figure 13**. During this process, while we have an increase of the rotor speed and load corresponding to the

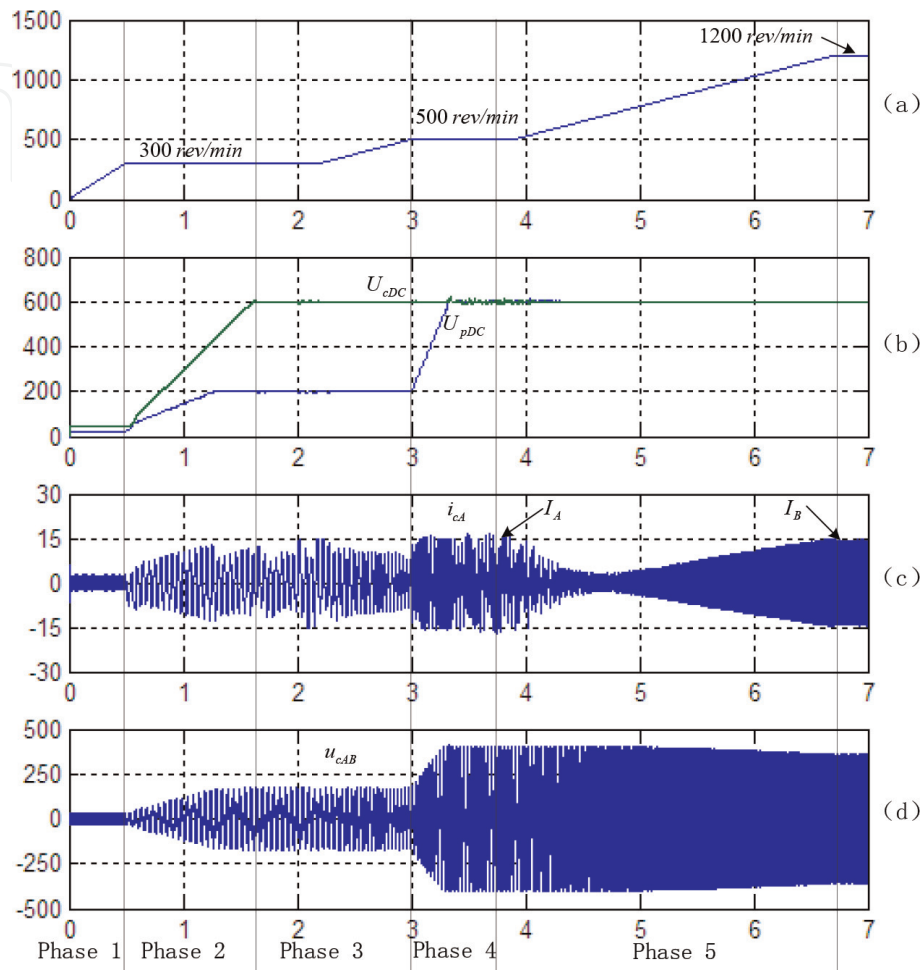


Figure 13. Simulation results of six-phase/three-phase DSWIG wind power system based on the optimal capacitor (62 μ F). (a) The rotor speed n . (b) The dc bus voltage U_{cDC} and U_{pDC} . (c) The line current of control winding i_{cA} . (d) The line-to-line voltage of control winding u_{cAB} .

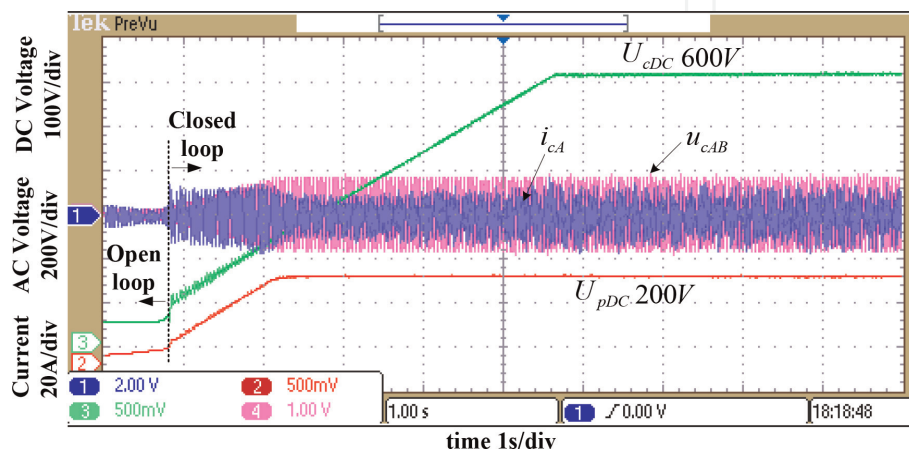


Figure 14. Experimental waveform of the DSWIG wind power system voltage buildup.

power curve, the control winding line current i_{cA} rms value shifts from negative to positive slope, the control winding current at low speed with light load (500 rev/min 4 kW) becomes equal with the value obtained during high speed with rated load regime (1200 rev/min 18 kW), which obeys to the equation $|I_C| = |I_E|$, and the rms value is about 10 A.

The rms value of control winding line current does not exceed over 10 A throughout the whole process, as shown in **Figure 14**, which entitles us to say that it is possible to further adjust the capacitor in order to get the capacity optimal through minimization of SEC for DSWIG wind power system with rectifier load.

6.2 Experimental results

The optimal selection algorithm and simulation were performed previously, followed by the experimental work. The experiments were carried out using an 18 kW six-phase/three-phase DSWIG wind power system prototype. The control software is soft coded in a Freescale MC56F8346 DSP-based development system. A three-leg Mitsubishi intelligent power module (IPM) is used for the buildup of the static excitation converter. The wind turbine dynamics will be emulated by a 20 kW three-phase induction motor driven by a Siemens M440 inverter. The excitation capacitor value is selected at $60\mu F$.

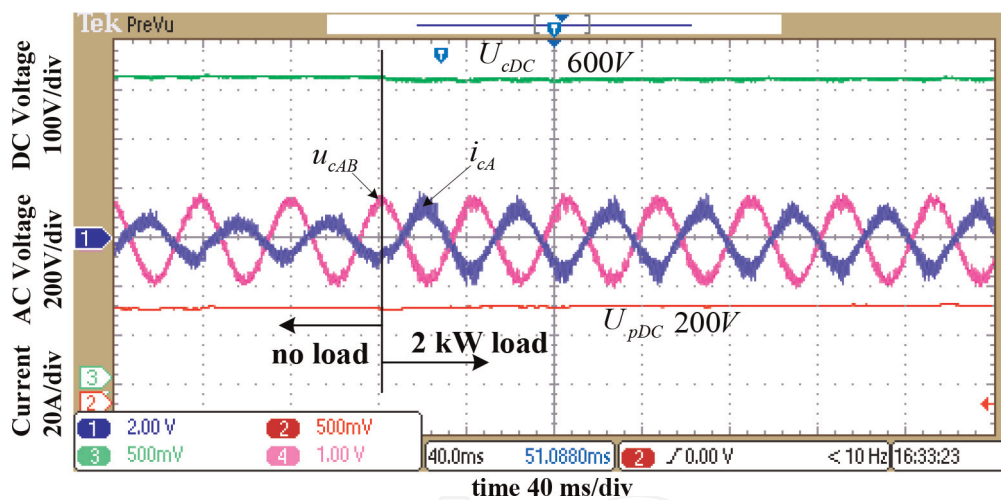


Figure 15. Experimental waveform at 450 rev/min with 2 kW when the DSWIG outputs power from the control winding at low speed.

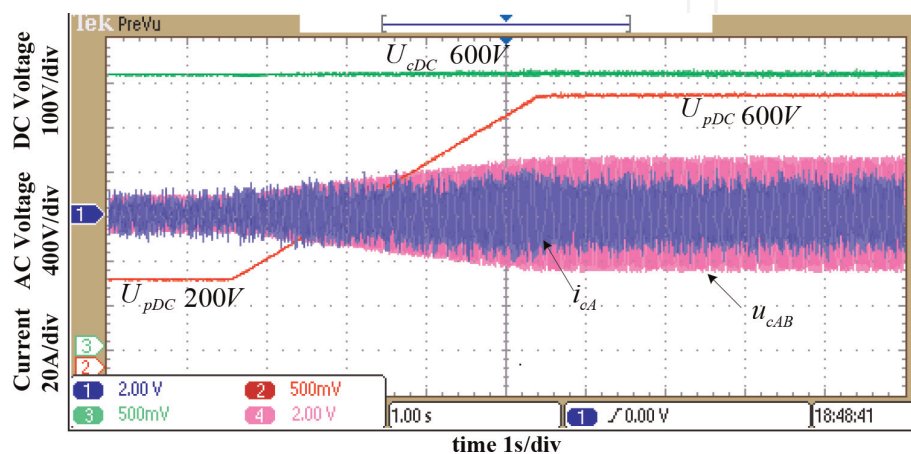


Figure 16. Experimental waveform of the transition at 500 rev/min.

When the turbine shaft rotates at a minimum speed of 300 rev/min, the system begins to build up voltage. The experimental results for this stage with the control strategy described above have been shown in **Figure 14**. It can be noticed that U_{pDC} and U_{cDC} rises with constant pace up to 200 and 600 V, respectively, without any overshoot in voltage and current.

According to the theoretical analysis presented earlier above, when the speed is in the range of low wind speed, the rotor speed is low and the output power is small. In this case, the generated power is transferred through the SEC from the control

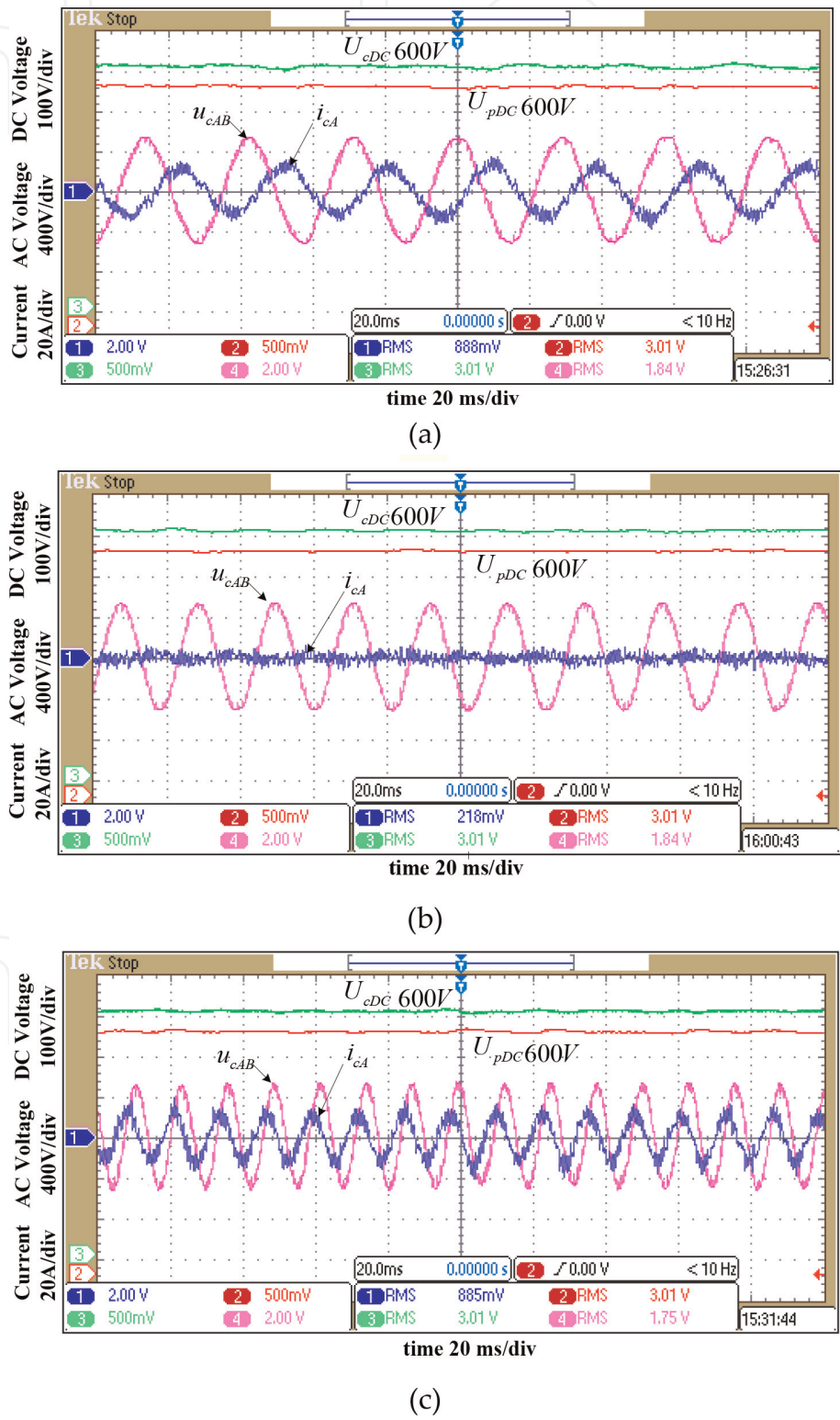


Figure 17. DC bus voltage waveforms of the control winding line-to-line voltage and line current of DSWIG wind power system when the speed is increasing from 500 to 1200 rev/min. (a) Light load, 3.5 kW 500 rev/min, (b) 11 kW, 710 rev/min, (c) rated load, 18 kW, 1200 rev/min.

winding. **Figure 15** presents the experimental tests showing the characteristic waveform of the DSWIG wind power system spinning at 450 rev/min with 2 kW electric load. In this case, the rms value of control winding line current is about 8.5 A.

The power winding voltage U_{pDC} is controlled from 200 to 600 V when the speed reaches 500 rev/min. The speed modification is followed by a change of the line-to-line voltage and line current of control winding. Through this transient state, U_{cDC} is preserved at 600 V constant. The experimental test results show the transient state waveform of the voltage shown in **Figure 16**.

Figure 17 depicts the experimental results indicating the control winding line-to-line voltage and line current following several typical operating points/states of the energization process ranging from 500 to 1200 rev/min. In **Figure 17a**, one may notice that the line current is phase shifted behind the line-to-line voltage no $< 120^\circ$ (it is phase shifted behind the phase voltage almost 90° electrical degrees), which indicates that the SEC will provide the reactive excitation power to the generator and the rms value is 8.9 A. In a similar way, while the speed increases, the load of the generator accelerates. When the speed grows to 710 rev/min, the output power of the generator is close to 11 kW.

The reactive current provided by SEC in this situation is irrelevant, close to zero as it can be seen from **Figure 17b**. This can be explained by the fact that enough reactive excitation power required by the generator is provided by the excitation capacitor. The reactive excitation power provided by excitation capacitor decreases below the generator demand, while the speed and load are slowly increasing. This is the situation when the SEC must extract the supplementary reactive excitation power from the generator output. Over 800 rev/min, the generation system will be capable to provide the rated power. The control winding line current and the corresponding line-to-line voltage waveforms when the speed is 1200 rev/min with 18 kW load are illustrated in **Figure 17c**. In this figure, the line current is phase shifted from the line-to-line voltage by 60° (it is ahead of the phase voltage for about 90°). The control winding current of is about 8.8 A (the rms value).

The experimental results in **Figure 18a** presents the direct relationship between the rotor speed and output power of the DSWIG wind power system.

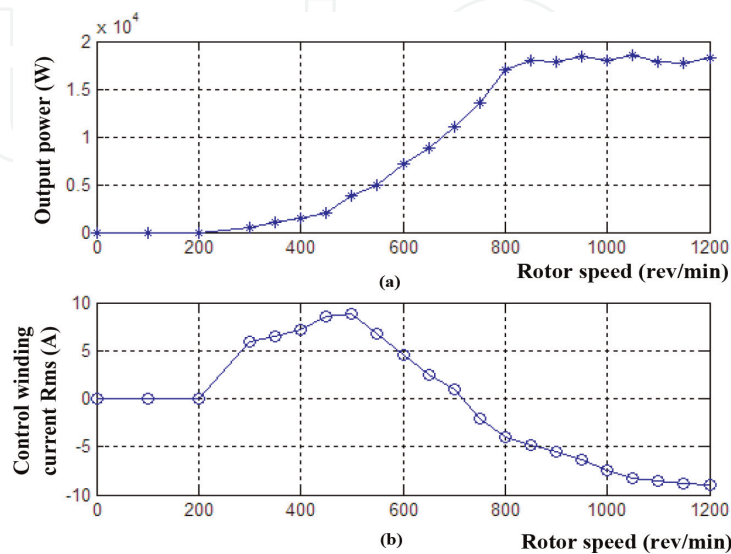


Figure 18. Experimental results for output power and control winding line current of DSWIG wind power system from 300 to 1200 rev/min. (a) Output power versus rotor speed. (b) Control winding line current versus rotor speed.

Figure 18b, in a similar fashion, shows the modification of the control winding line current rms value during the generator transient regime. It can be noticed that the rms value of minimal negative current approximately equals to the maximum positive value, which is in correspondence with the theoretical analysis and simulation results. Furthermore, it is obvious that the maximum capacity of SEC is about 1/3 of the rated output power. This is demonstrated by the experimental results, and the objective for a compact implementation of SEC is attained, which can lead to a reduction in the cost and size for the DSWIG wind power system.

7. Conclusions

In this chapter, novel dual stator-winding induction wind power generator system and its the optimal sizing algorithm of the excitation capacitor are presented. The work done here indicates that selection of optimal excitation capacitor value is highly dependent on generator parameters, speed range, and load but also is affected by the wind turbine power curve. Several methods are used to achieve the optimal excitation capacitor selection in order to reach the objective of minimizing the capacity of SEC.

We were using a complete model in the stator-voltage-orientation synchronous d-q frame. Through the analysis of the model of SEC, the coupling between the d and q axes of the DSWIG is underlined. Accordingly, a decoupling control strategy using the SVM is implemented at the level of hardware control. On the bases of this observation, the simulations and experiments from the prototype are carried out for verification. The results demonstrate the accuracy and soundness of this optimization algorithm for the DSWIG wind power system.

In this chapter, an optimal scheme is studied mainly, and it concentrates on the condition when relative parameters of the generator are identified. Additionally, the optimal design for the whole system including the generator should also be acknowledged. However, the optimization scheme obtained in this paper is rather a first attempt to the problem of topology design of multiphase induction machine-based generators and system optimization of the DSWIG system applied in wind power system.

Appendices and nomenclature

The six-phase/three-phase DSWIG parameters (both the rotor and control windings are converted to the power winding):

$$R_p = 0.624\Omega; R'_c = 0.434\Omega; R'_r = 0.32\Omega; L_{lp} = 3.26\text{mH}; L'_{lr} = 2.02\text{mH}; \\ L'_{lc} = 3.12\text{mH}; L_m = 92.4\text{mH}; L_{lmp12} = L_{lmcp1} = L_{lmcp2} = 0.42\text{mH}.$$

Rated power: 18 kW.

Rated speed: 750 rev/min.

Pole pairs: 4.

Rated DC output voltage: 600 V.

Filter inductor: $3 \times 4\text{mH}$.

Excitation capacitor: $6 \times 60\mu\text{F}$.

DC bus capacitor: $1100\mu\text{F}/900\text{V}$.

Interphase reactor: 9 mH.

Voltage of battery: 48 V.

IntechOpen

IntechOpen

Author details


Sorin Ioan Deaconu^{1*}, Feifei Bu², Marcel Topor¹, Lucian Nicolae Tutelea¹
and Nicolae Muntean¹

1 Politehnica University Timisoara, Romania

2 University of Aeronautics and Astronautics, Nanjing, China

*Address all correspondence to: sorin.deaconu@fih.upt.ro

IntechOpen

© 2019 The Author(s). Licensee IntechOpen. This chapter is distributed under the terms of the Creative Commons Attribution License (<http://creativecommons.org/licenses/by/3.0>), which permits unrestricted use, distribution, and reproduction in any medium, provided the original work is properly cited. 

References

- [1] Global Wind Energy Council. Global Wind Statistics 2012. 2013
- [2] Chen W, Huang AQ, Li C, Wang G, Gu W. Analysis and comparison of medium voltage high power DC/DC converters for offshore wind energy systems. *IEEE Transactions on Power Electronics*. 2013;**28**(4):2014-2023
- [3] Prasai A, Yim J, Divan D, Bendre A, Sul S. A new architecture for offshore wind farms. *IEEE Transactions on Power Electronics*. 2008;**23**(3): 1198-1204
- [4] Kirby NM, Xu L, Luckett M, Siepmann W. HVDC transmission for large offshore wind farms. *Power Engineering Journal*. 2002;**16**(3):135-141
- [5] Li H, Chen Z. Overview of different wind generator systems and their comparisons. *IET Renewable Power Generation*. 2008;**2**(2):123-138
- [6] Echenique E, Dixon J, Cardenas R, Pena R. Sensorless control for a switched reluctance wind generator based on current slopes and neural networks. *IEEE Transactions on Industrial Electronics*. 2009;**56**(3): 817-825
- [7] Leijon M, Dahlgren M, Walfridsson L, Li M, Jaksts A. A recent development in the electrical insulation systems of generators and transformers. *IEEE Electrical Insulation Magazine*. 2001;**17**(3):10-15
- [8] Egea-Alvarez A, Bianchi F, Junyent-Ferre A, Gross G, Gomis-Bellmunt O. Voltage control of multiterminal VSC-HVDC transmission systems for offshore wind power plants: Design and implementation in a scaled platform. *IEEE Transactions on Industrial Electronics*. 2013;**60**(6):2381-2391
- [9] Muyeen SM, Takahashi R, Tamura J. Operation and control of HVDC-connected offshore wind farm. *IEEE Transactions on Sustainable Energy*. 2010;**1**(1):30-37
- [10] Bozhko SV, Blasco-Gimenez R, Li R, Clare JC, Asher GM. Control of offshore DFIG-based wind farm grid with line-commutated HVDC connection. *IEEE Transactions on Energy Conversion*. 2007;**22**(1):71-78
- [11] Bansal RC, Bhatti TS, Kothari DP. Bibliography on the application of induction generators in nonconventional energy systems. *IEEE Transactions on Energy Conversion*. 2003;**18**(3):433-439
- [12] Hu Y, Huang W, Li Y. A novel instantaneous torque control scheme for induction generator systems. *IEEE Transactions on Energy Conversion*. 2010;**25**(3):795-803
- [13] Zhang J, Rahman MF. A direct-flux-vector-controlled induction generator with space-vector modulation for integrated starter alternator. *IEEE Transactions on Industrial Electronics*. 2007;**54**(5):2512-2520
- [14] Leidhold R, Garcia G, Valla MI. Induction generator controller based on the instantaneous reactive power theory. *IEEE Transactions on Energy Conversion*. 2002;**17**(3):368-373
- [15] Ojo O, Davidson IE. PWM-VSI inverter-assisted stand-alone dual stator winding induction generator. *IEEE Transactions on Industry Applications*. 2000;**36**(6):1604-1611
- [16] Wang D, Ma W, Xiao F, Zhang B, Liu D, Hu A. A novel stand-alone dual stator-winding induction generator with static excitation regulation. *IEEE Transactions on Energy Conversion*. 2005;**20**(4):826-835
- [17] Li Y, Hu Y, Huang W, Liu L, Zhang Y. The capacity optimization for

the static excitation controller of the dual-stator-winding induction generator operating in a wide speed range. *IEEE Transactions on Industrial Electronics*. 2009;**56**(2):530-541

[18] Bu F, Huang W, Hu Y, Shi K. An excitation-capacitor-optimized dual stator-winding induction generator with the static excitation controller for wind power application. *IEEE Transactions on Energy Conversion*. 2011;**26**(1): 122-131

[19] Liu L, Hu Y, Huang W. Optimal design of dual stator-winding induction generator with variable speed based on improved genetic algorithm. In: 2005 The 8th International Conference on Electrical Machines and Systems, ICEMS. 2005. pp. 2343-2348

[20] Zhu W, Wang X, Wang X. Optimal wind power capturing operational mode of a variable-speed variable-frequency wind power generation system. *Automation of Electric Power Systems (China)*. 2009;**33**(11):94-98

[21] Koutroulis E, Kalaitzakis K. Design of a maximum power tracking system for wind-energy-conversion applications. *IEEE Transactions on Industrial Electronics*. 2006;**53**(2): 486-494

[22] Li Y, Hu Y, Liu L, Huang W, Chen G. Control of a novel dual stator-winding induction generator for wide speed-range operation. In: *IEEE Power Electronics Specialists Conference*. 2007. pp. 2096-2101

[23] Hu Y, Huang W, Zhang L. Research on employing starter/generator system. *Transactions of China Electrotechnical Society*. 2006;**2**(5):7-13

[24] Peng F, Lai J. Generalized instantaneous reactive power theory for three-phase power systems. *IEEE Transactions on Instrumentation and Measurement*. 1996;**45**(1):293-297

[25] Li Y, Hu Y, Huang W, Qiu J, Chen G, Hao Z. Voltage control of dual stator-winding induction generator system using space vector modulation. *Proceedings of Chinese Society Electrical Engineering*. Aug 2008;**28** (23):112-118